

Sliding Mode Tracking Control of Surface Vessels¹

Hashem Ashrafiuon and Kenneth R. Muske

Center for Nonlinear Dynamics and Control, Villanova University, Villanova, PA 19085

Abstract—A sliding mode control law is presented and experimentally implemented for trajectory tracking of underactuated autonomous surface vessels. The control law is developed by introducing a first order sliding surface in terms of surge tracking errors and a second order one in terms of lateral motion tracking errors. The resulting sliding mode control law guarantees position tracking while the rotational motion remains bounded. The vessel is a small boat with two propellers in a small indoor pool. The position and orientation of the boat is measured using a camera and with two infrared diodes attached near the front and back ends of the boat. A computer with controller board processes the camera image, calculates the control forces and their corresponding input voltages, and sends the control signals to wireless receivers on the vessel using a wireless transmitter. Several experiments are performed where the vessel follows straight-line trajectories fairly accurately.

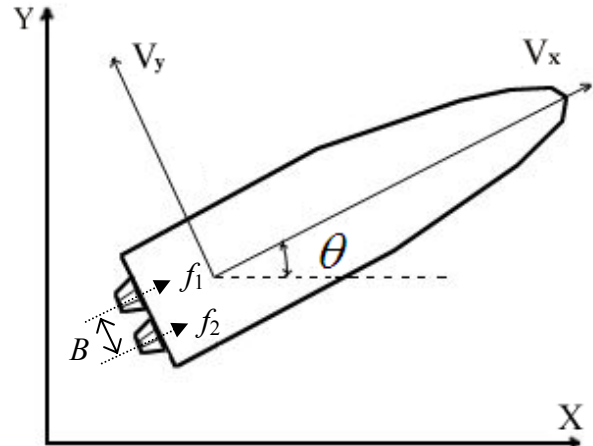


Fig. 1. Planar model of a surface vessel with two propellers

I. INTRODUCTION

Autonomous surface vessels with two actuator inputs are considered as underactuated mechanical systems since they possess three DOF when modeled as a single planar rigid body. Position control of underactuated systems has received increased attention in the last decade with most of the research focusing on feedback linearization, backstepping, controlled Lagrangian, and sliding mode control methods. Application of underactuated control to ocean vehicles includes hovercraft [1], autonomous underwater vehicles [2-4], and surface vessels [5-22]. This research may also be divided into set point [5-10] and trajectory tracking [11-22] position control problems since the respective controllers are very different. The only experimental work in the underactuated surface vessel control area, to our knowledge, have been presented for set point stabilization [10] and ship tracking [20].

In this work, we address the trajectory tracking control problem of autonomous surface vessels. Equations of motion representing the planar model of a three DOF vessel with two propellers are presented using a nonlinear hydrodynamic damping model. Based on this model, an asymptotically stable trajectory tracking sliding mode control law is developed using two sliding surfaces for calculation of the two propeller forces. The first one is a first order surface comprised of position and velocity tracking errors of the surge motion. The second surface is a second order one defined in terms of the vessel's lateral position, velocity, and

acceleration tracking errors. It is assumed that only the absolute position and orientation of the vessel are measured and available for feedback as is the case when a Global Positioning System or a camera is used. Hence, the absolute velocities are numerically estimated and surge and lateral velocities are calculated through kinematic relations.

The experimental setup includes a small boat with two LED's (Light Emitting Diodes) and two propellers in a small indoor pool, camera, capture card, computer, dSpace card, wireless transmitters and receivers, and two DC motors with custom designed planetary gear trains. The motion of the two LED's are captured and filtered to determine the location and orientation of the vessel [22]. The input voltages are estimated through interpolation of the calculated control forces and converted to analog signals by Real Time Workshop and the dSpace card. The signals are wired to a wireless transmitter, which in turn transmits them to DC motor controller receivers. Several experiments are performed where the vessel successfully follows straight-line trajectories.

II. MODEL

Figure 1 shows the model of a planar surface vessel with two propellers inputs f_1 and f_2 . The geometrical relationship between the inertial reference frame and the vessel-based body-fixed frame is defined in terms of velocities as:

$$\begin{aligned} \dot{x} &= v_x \cos\theta - v_y \sin\theta \\ \dot{y} &= v_x \sin\theta + v_y \cos\theta \\ \dot{\theta} &= \omega \end{aligned} \quad (1)$$

¹ This research was partially supported by the Office of Naval Research under the ONR Grant number N00014-04-1-0642.

where (x, y) denote the position of the center of mass and θ the orientation angle of the vessel in the inertial reference frame. While, (v_x, v_y) and ω are linear and angular velocities of the vehicle in the body-fixed frame, respectively.

In the body-fixed frame, the nonlinear equations of motion for a simplified model of the dynamics of a surface vessel, where motions in heave, roll, and pitch are neglected, are given by:

$$\begin{aligned} m_{11}\dot{v}_x - m_{22}v_y\omega + d_1v_x^{\alpha_1} &= f \\ m_{22}\dot{v}_y + m_{11}v_x\omega + d_2v_y^{\alpha_2} &= 0 \\ m_{33}\dot{\omega} + m_dv_xv_y + d_3\text{sgn}(\omega)|\omega|^{\alpha_3} &= T \end{aligned} \quad (2)$$

Note that, we only consider forward vessel motion in this work since the reverse motion dynamics can be quite different, i.e. $v_x, v_y > 0$. The mass and nonlinear damping parameters $(m_{ii}, d_i, \alpha_i, i=1, 2, 3)$ are assumed to be constant where $m_{11} \neq m_{22}$ due to the added mass effects [23] and $m_d = m_{22} - m_{11}$. Assuming the propellers are symmetrically located apart at a lateral distance B , the surge control force f and the yaw control moment T are given by:

$$f = f_1 + f_2, \quad T = (f_1 - f_2)B/2 \quad (3)$$

III. SLIDING MODE CONTROL LAW

In the sliding mode control approach [24], we define asymptotically stable surfaces (\mathcal{S}) such that all system trajectories converge to these surfaces in finite time and slide along them until they reach their desired destination at their intersection. The reaching conditions are established by defining $\frac{1}{2}\mathcal{S}^T\mathcal{S}$ as the Lyapunov function and ensuring that for each surface i :

$$S_i\dot{S}_i \leq -\eta_i|S_i|, \quad \eta_i > 0 \quad (4)$$

where the value of constant η_i determines how fast the trajectory will reach surface i .

A. Surge Control Law

In the case of underactuated surface vessels, we define two surfaces to determine the two control inputs. The first sliding surface is a first order one defined in terms of the vessel's surge motion tracking errors:

$$S_1 = \tilde{v}_x + \lambda_1 \int_0^t \tilde{v}_x(\tau) d\tau \quad (5)$$

where “ \sim ” is used to denote the difference between the actual and desired values; i.e. $\tilde{v}_x = v_x - v_{xd}$. Note that the integral of v_x is used since surge position is undefined. The

desired motion is specified in the inertial reference frame and is related to the desired surge and lateral velocity and acceleration as:

$$\begin{aligned} v_{xd} &= \cos \theta \dot{x}_d + \sin \theta \dot{y}_d \\ \dot{v}_{xd} &= \cos \theta \ddot{x}_d + \sin \theta \ddot{y}_d + v_{yd} \omega \end{aligned} \quad (6)$$

$$\begin{aligned} v_{yd} &= -\sin \theta \dot{x}_d + \cos \theta \dot{y}_d \\ \dot{v}_{yd} &= -\sin \theta \ddot{x}_d + \cos \theta \ddot{y}_d - v_{xd} \omega \end{aligned} \quad (7)$$

Taking the time derivative of the surface and using the first of Eq. (2), the surge control input can be determined as:

$$f = -\hat{m}_{22}v_y\omega + \hat{d}_1v_x^{\alpha_1} - \hat{m}_{11}\dot{S}_{r1} - k_1\text{sgn}(S_1) \quad (8)$$

$$k_1 = M_{22}|v_y\omega| + D_1v_x^{\alpha_1} + M_{11}|\dot{S}_{r1}| + \hat{m}_{11}\eta_1 \quad (9)$$

where “ $\hat{\cdot}$ ” is used to indicate our estimated model parameters and functions, $\dot{S}_{r1} = -\dot{v}_{xd} + \lambda_1\tilde{v}_x$, and M_{ii} & D_i indicate the error bounds for estimated values of m_{ii} & d_i , respectively.

B. Lateral Motion Control Law

We define the second sliding surface as a second-order one in terms of the vessel's lateral motion tracking errors:

$$S_2 = \tilde{v}_y + 2\lambda_2\tilde{v}_y + \lambda_2^2 \int_0^t \tilde{v}_y(\tau) d\tau \quad (10)$$

Taking the time derivative of the second surface requires the calculation of actual and desired \dot{v}_y . Hence, we take the time derivative of the lateral equation of motion in Eq. (2) and substitute for the accelerations from the surge and yaw equations to calculate the yaw moment control:

$$\begin{aligned} T = \frac{\hat{m}_{33}}{v_{xd} - \hat{m}_r v_x} \left[\left(\frac{\omega}{\hat{m}_{22}} \right) f - \hat{v}_r - \hat{v}_{rd} \right. \\ \left. - \dot{S}_{r2} - k_2 \text{sgn}(S_2) \right] \end{aligned} \quad (11)$$

$$\begin{aligned} k_2 = (b_{gm} - 1) \left| \left(\frac{\omega}{\hat{m}_{22}} \right) f - \hat{v}_r - \hat{v}_{rd} - \dot{S}_{r2} \right| \\ + b_{gm} [V_r + V_{rd} + |f_x\omega|\Delta + \eta_2] \end{aligned} \quad (12)$$

where

$$\begin{aligned} v_r = \frac{d_1\omega v_x^{\alpha_1}}{m_{22}} + \frac{m_r d_2 \omega v_x v_y^{\alpha_2 - 1}}{m_{22}} + \frac{d_2^2}{m_{22}^2} v_y^{2\alpha_2 - 1} \\ + \frac{m_{11} d_3 v_x \text{sgn}(\omega) |\omega|^{\alpha_3}}{m_{33}} - \omega^2 v_y + \frac{m_r m_d}{m_{33}} v_x^2 v_y \end{aligned} \quad (13a)$$



Fig. 2. The vessel with DC motors, receivers, gearboxes, and couplers

$$v_{rd} = s\theta(\ddot{x}_d + 2\dot{y}_d\omega) - c\theta(\ddot{y}_d - 2\dot{x}_d\omega) + v_{yd}\omega^2 - \frac{v_{xd}}{m_{33}}(m_d v_x v_y + d_3\omega^{\alpha_3}) \quad (13b)$$

$$\dot{S}_{r2} = 2\lambda\dot{\tilde{v}}_y + \lambda^2\tilde{v}_y \quad (13c)$$

In the above equations, $m_r = \frac{m_{11}}{m_{22}}$, and V_r , V_{rd} and Δ are the error bounds for v_r , v_{rd} , and $1/m_{22}$, respectively. Also, b_{gm} is the geometric mean of the parameter b defined as:

$$b = \frac{m_{22}v_{xd} - m_{11}v_x}{m_{22}m_{33}}, \quad b_{gm} = \left(\frac{b_{\max}}{b_{\min}}\right)^{1/2} \quad (14)$$

where b_{\max} and b_{\min} are defined based on uncertainty in mass elements.

C. Stability Analysis

The surge force and yaw moment control laws in Eqs. (8) and (11), respectively, are derived based on the reaching conditions in Eq. (4) and hence guarantee that the trajectory reaches both surfaces in finite time. Furthermore, the two surfaces in Eqs. (5) and (10) are asymptotically stable. Hence the trajectory exponentially slides to the origin at the intersection of the two surfaces. Since

\tilde{v}_x , $\int_0^t \tilde{v}_x(\tau)d\tau$, \tilde{v}_y , and $\int_0^t \tilde{v}_y(\tau)d\tau \rightarrow 0$, the kinematic relations in Eq. (1) also guarantee trajectory tracking in the inertial reference frame.

We also propose that the vessel yaw motion, ω , is BIBO stable. Let us define the Lyapunov candidate function

$$V = \frac{1}{2}m_{33}\omega^2 > 0 \quad (15)$$

Using Eq. (2), the time derivative of V may be written as:

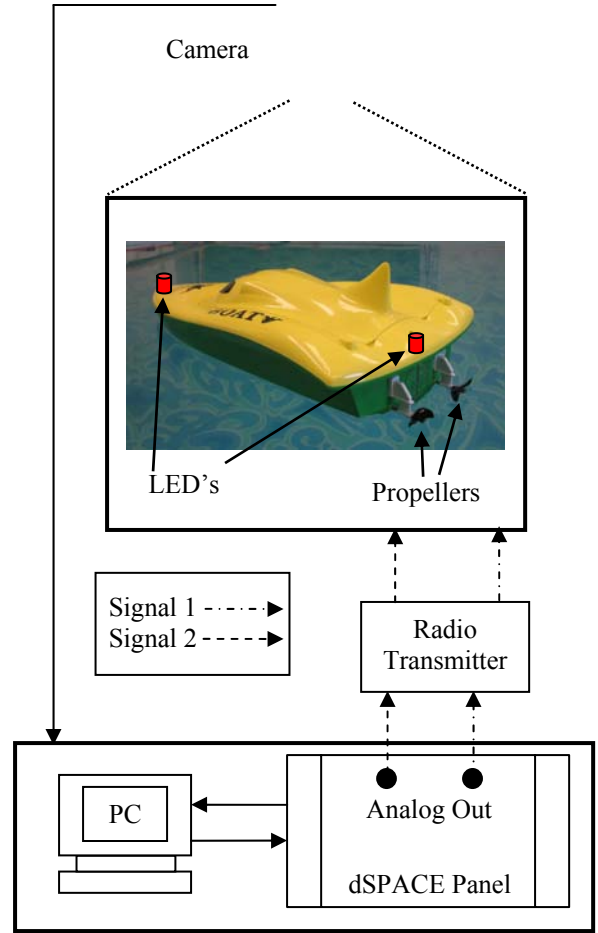
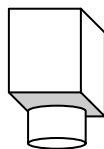


Fig. 3. Diagram of the experimental setup

$$\begin{aligned} \dot{V} &= \omega[T - m_d v_x v_y - d_3 \operatorname{sgn}(\omega)|\omega|^{\alpha_3}] \\ &= \omega(T - m_d v_x v_y) - d_3 |\omega|^{1+\alpha_3} \end{aligned} \quad (16)$$

Hence, $\dot{V} < 0$ if $d_3 |\omega|^{\alpha_3} > (T - m_d v_x v_y)$ and since T , v_x , and v_y are bounded then ω remains bounded.

IV. EXPERIMENTAL SETUP

The experiments are performed with a small 20-in, 1.614 kg boat in a 6ft x 8ft indoor pool. Two DC motors are used and mounted to propeller shafts using in-house couplings (Fig. 2). The propellers are 7 cm apart ($B = .07$ m). Since our DC motors are only controllable in a high-speed range, we have reduced their speed at 1:16 ratio with custom designed planetary gear trains. The motors were originally controlled using a joystick and wireless receivers. However, we have modified the joystick such that the signals can be transmitted from a dSpace board with the help of two power supplies (not shown) which are only used to shift the voltage range such that both forward and reverse propeller motion can be produced.

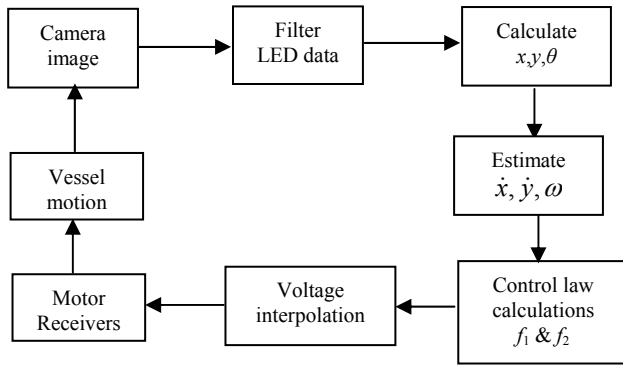


Fig. 4. Block diagram of implementation of the feedback control law

We have used a digital black and white camera for our feedback measurements. Two infrared LED's are installed near the front and back ends of the centerline of the vessel. The camera is installed 6 ft above the center of the pool and captures the image of the whole pool area. The infrared images are then filtered out and used to calculate the position of the center of gravity of the boat and its orientation. The camera rate is 30 frames per second. A diagram of the experimental setup is shown in Fig. 3.

Since the camera image is distorted and in the form of an image matrix, we had to calibrate the camera. We placed a board on the top of the pool and installed infrared LED's at known locations all over its surface. We then captured an image and filtered out the LED locations on the image matrix. Two dimensional cubic interpolation functions were used to fit the image matrix. We used these data to interpolate and find the position of the two infrared LED's attached to the vessel during the experiments. The absolute position of the vessel (x, y) and its orientation (θ) are calculated from the LED data. Note that, the LED's are installed at the top of two plastic columns such that they are at the same height of the grid used for cameral calibration.

We have not modeled the actuator dynamics in this work. Instead, we determined a relationship between motor input voltage and propeller force by applying several constant voltages to the motors, capturing the ensuing motion, and comparing them with our model simulation results. As a result of these experiments, we found simple parabolic force-voltage relationships at voltages larger than .2 V in positive and .3 V in the negative/reverse directions. In other words, the dead-band of the motors was between -.3 V and .2 V. Though the motors are not perfectly balanced, we assumed the two motor force-voltage relations are identical. We have limited the input voltages to ± 1 V to avoid damaging the gearboxes.

The block diagram in Fig. 4 illustrates the implementation of the control law through camera data filtering and calibration, velocity estimation using the camera position data feedback, and propeller force - motor input voltage interpolation. Both camera and motor calibration results are presented in a separate paper.

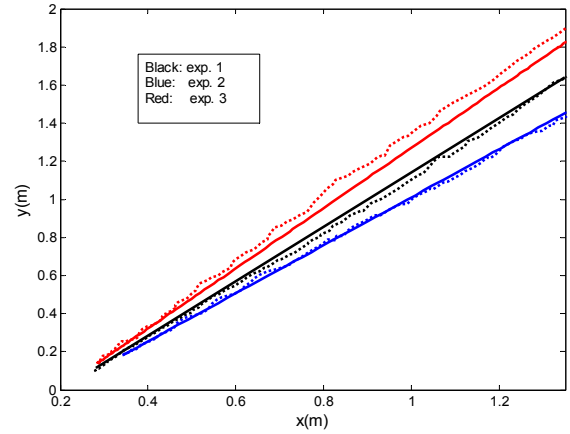


Fig. 5. Desired versus actual vessel path during three experiments; solid lines indicate desired and dotted line indicate actual values

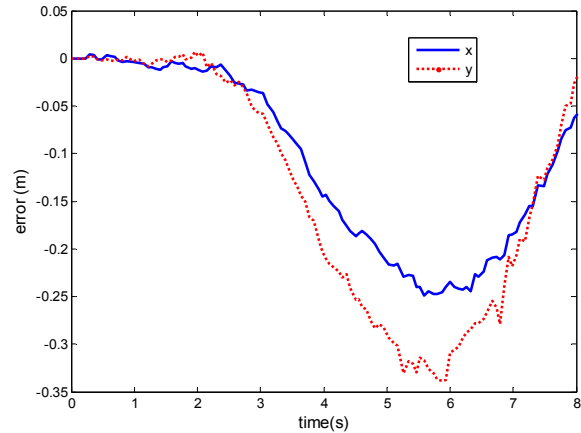


Fig. 6. Trajectory tracking error for a typical straight-line experiment

V. RESULTS

We performed a series of vessel surge, lateral and yaw motion by applying various known constant forces and moments through a pulley system to estimate the parameters of the model presented in Eq. (2). These experiments are not the subject of this paper and are presented in a separate article. The model data and their uncertainty in SI units for our small vessel are:

$$\begin{aligned}
 m_{11} &= 1.956 \pm .019 & m_{22} &= 2.405 \pm .117 & m_{33} &= .043 \pm .0068 \\
 d_1 &= 2.436 \pm .023 & d_2 &= 12.992 \pm .297 & d_3 &= .0564 \pm .00085 \\
 \alpha_1 &= 1.510 \pm .0075 & \alpha_2 &= 1.747 \pm .013 & \alpha_3 &= 1.592 \pm .0285
 \end{aligned}$$

The selected control law parameters are:

$$\lambda_1 = .5, \lambda_2 = .5, \eta_1 = .01, \eta_2 = .01, \phi_1 = .1, \phi_2 = .1,$$

where the discontinuous “sign” functions have been replaced with continuous saturation functions of boundary layer thicknesses ϕ_1 and ϕ_2 ; i.e., $\text{sgn}(S_i) \approx \text{sat}(\frac{S_i}{\phi_i})$, $i = 1, 2$

to avoid chattering. The vessel is commanded to follow a straight-line for 8 seconds starting from rest at one corner of the pool and stopping near the opposite corner.

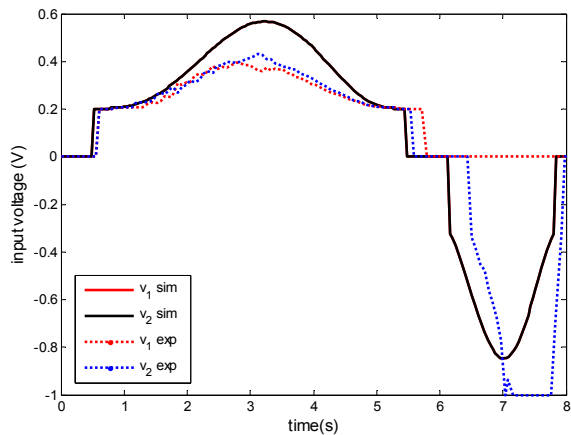


Fig. 7. Comparison of Applied voltages during the experiment and simulation

Figure 5 shows the actual paths followed by the vessel are very close to the desired straight-line paths in a series of experiments. The controller is very robust particularly since the pool water was visibly wavy during these experiments. Though the path error was very small, the vessel's trajectory error in x and y directions were much larger, as shown in Fig. 6. It seems that while the boat is accelerating or cruising it falls behind the trajectory. However, the vessel compensates during the decelerations phase the errors become much smaller again. This suggests that the interpolation process underestimates the input voltage for the positive propeller motion and hence smaller voltages result in slower vessel motion. Figure 7 shows the heading angle during a typical experiment is not constant but remains bound.

Figure 8 presents the input voltages for the two motors during a typical straight-line experiment and simulation. It can be observed that, in the experiment, the applied voltages during the positive propeller motion are smaller. Another interesting phenomenon is that the vessel must maintain a constant heading angle to go straight. However, after nearly 7 seconds, its heading has deviated about 15° CW. This explains why after 7 seconds, one motor requires maximum reverse input voltage while the other requires no input and the heading angle deviation is somewhat compensated for during the last second of experiment.

There are several sources of error in this experiment including camera calibration error, large sample time (.04 s) due to camera limitation and real time image processing, motor calibration error, lack of speed control at low voltages, and imbalances between the two motors. The main cause of error at the moment is due to the three latter sources. Motor calibration is not very accurate since it is based on simple experiments and comparison with model simulation. Also, the two propellers must rotate in opposite direction to provide good performance. However, our motor speed controller hardware does not perform the same in both directions and hence equal voltages do not produce the same exact motor speeds in many of our experiments.

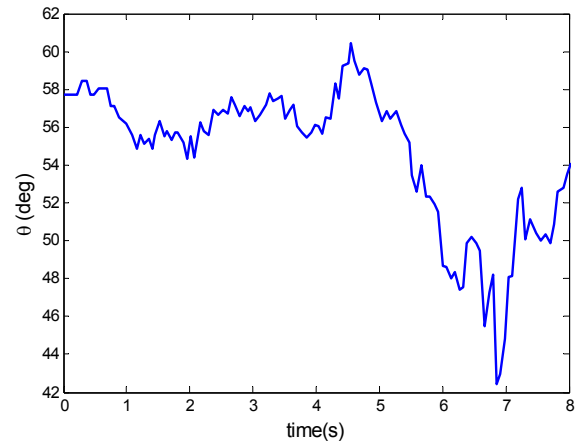


Fig. 8. Vessel's heading angle during a typical straight-line experiment

VI. CONCLUSION

A sliding mode control law was presented, implemented, and tested experimentally. The control law was developed using a first order surface in terms of the surge tracking errors and a second order surface in terms of the lateral tracking errors. The vessel absolute position and orientation were measured using a camera following two LED's on the vessel. The motor input voltages were estimated from the controller propeller forces and transmitted to the motors using wireless transmitters and receivers. Several straight-line experiments were successfully performed. Future work will include experiments with other trajectories, further improvements in the experimental setup, and coordinated control of multiple vessels.

VII. ACKNOWLEDGEMENTS

We would like to thank and acknowledge the help of our undergraduate students, Timothy Flynn, Geoffrey Haas, and Ryan McCloskey and our graduate student Reza Soltan of the College of Engineering at Villanova University, for setting up the experiments, troubleshooting, and helping with the programming. Support for this work from the Center for Nonlinear Dynamics and Control (CENDAC) at Villanova University is also acknowledged.

REFERENCES

- [1] Fantoni, I., Lozano, R., Mazenc, F., and Pettersen, K.Y., "Stabilization of a nonlinear underactuated hovercraft", *Proceedings of the IEEE Conference on Decision and Control*, v 3, 1999, p 2533-2538.
- [2] Leonard, N.E., "Control synthesis and adaptation for an underactuated autonomous underwater vehicle", *IEEE Journal of Oceanic Engineering*, v 20, n 3, 1995, p 211-220.

- [3] Peterson, K.Y. and Egeland, O., "Time-varying exponential stabilization of the position and attitude of an underactuated autonomous underwater vehicle," *IEEE Transactions on Automatic Control*, v 44, n 1, 1999, p 112-15.
- [4] Aguiar, A.P., and Pascoal, A.M., "Dynamic positioning and way-point tracking of underactuated AUVs in the presence of ocean currents", *41st IEEE Conference on Decision and Control. Proceedings (Cat. No.02CH37375)*, v 2, 2002, p 2105-2110.
- [5] Reyhanoglu, M., "Exponential stabilization of an underactuated autonomous surface vessel", *Automatica*, v 33, n 12, 1997, p 2249-2254.
- [6] Kim, T.-H., Basar, T., and Ha, I.-J., "Asymptotic stabilization of an underactuated surface vessel via logic-based control" *American Control Conference*, 2002, p 4678 – 4683.
- [7] Mazenc, F., Pettersen, K., and Nijmeijer, H., "Global uniform asymptotic stabilization of an underactuated surface vessel," *IEEE Transactions on Automatic Control*, v 47, n 10, 2002, p 1759-1762.
- [8] Soro, D., and Lozano, R., "Semi-global practical stabilization of an underactuated surface vessel via nested saturation controller," *Proceedings of the American Control Conference*, Denver, CO, v 3, 2003, p 2006-2011.
- [9] Dong, W., and Guo, Y., "Global time-varying stabilization of underactuated surface vessel," *IEEE Transactions on Automatic Control*, v 50, n 6., 2005, p 859-864.
- [10] Peterson, K.Y., Mazenc, F., and Nijmeijer, H., "Global Uniform Asymptotic Stabilization of an Underactuated Surface Vessel: Experimental Results," *IEEE Transactions on Control Systems Technology*, v 12, n 6, 2004, p 891-903.
- [11] Indiveri, G., Aicardi, M., and Casalino, G., "Nonlinear time-invariant feedback control of an underactuated marine vehicle along a straight course", *Proceedings of 5th Conference on Maneuvering and Control of Marine Craft (MCMC 2000)*, Aalborg, Denmark, 2000.
- [12] Godhavn, J.-M., 1996, "Nonlinear Tracking of Underactuated Surface Vessels", *Proceedings of the IEEE Conference on Decision and Control*, Kobe, Japan, 2000.
- [13] Pettersen, K.Y., and Nijmeijer, H., "Tracking control of an underactuated surface vessel" *Proceedings of the IEEE Conference on Decision and Control*, 1998, p 4561-4566.
- [14] Encarnacao, P., and Pascoal, A., "Combined trajectory tracking and path following: An application to the coordinated control of autonomous marine craft," *40th IEEE Conference on Decision and Control (CDC)*, Orlando, FL, v 1, 2001, p 964-969.
- [15] Olfati-Saber, R., "Exponential epsilon -tracking and epsilon -stabilization of second-order nonholonomic SE (2) vehicles using dynamic state feedback," *Proceedings of the American Control Conference (IEEE Cat. No.CH37301)*, v 5, 2002, p 3961-3967.
- [16] Aguiar, A.P., and Hespanha, J.P., "Position tracking of underactuated vehicles," *Proceedings of the American Control Conference*, v 3, 2003, p 1988-1993.
- [17] Behal, A., Dawson, D. M., Dixon, W.E., and Fang, Y., "Tracking and regulation control of an underactuated surface vessel with nonintegrable dynamics," *IEEE Transactions on Automatic Control*, v 47, n 3, 2002, p 495-500.
- [18] Jiang, Z.-P., "Global tracking controller design for underactuated ships," *Proceedings of the IEEE Conference on Control Applications*, Mexico City, 2001, p 978-983.
- [19] Toussaint, G. J., Basar, T., and Bullo, F., "Tracking for nonlinear underactuated surface vessels with generalized forces," *Proceedings of the IEEE International Conference on Control Applications*, Anchorage, AK, v 1, 2000, p 355-360.
- [20] Lefeber, E., Pettersen, K. Y., and Nijmeijer, H., "Tracking control of an underactuated ship," *IEEE Transactions on Control Systems Technology*, v 11, n 1, 2003, p 52-61.
- [21] Ashrafiuon, H., and Ren, P., "Sliding mode tracking control of underactuated surface vessels," *Proceedings of the ASME IMECE*, 2005, paper no. IMECE2005-79276.
- [22] Nikkhah, M., and Ashrafiuon, H., "Robust Control of a Vessel Using Camera Feedback and Extended Kalman Filter," *ASME IMECE*, Nov. 5-10, 2006, Chicago, IL, paper no. IMECE2006-16164
- [23] Fossen, T. I., "Guidance and control of ocean vehicles," John Wiley & Sons, New York, NY, 1994, p 168-171.
- [24] Utkin, V. I., "Variable structure systems with sliding modes," *IEEE Transactions on Automatic Control*, v 22, 1977, p 212-222.